International Journal of GEOMATE, March., 2021, Vol.20, Issue 79, pp. 1-8
ISSN: 2186-2982 (P), 2186-2990 (O), Japan, DOI: https://doi.org/10.21660/2021.79.38620
Geotechnique, Construction Materials and Environment

# TENSILE BEHAVIOR AND STRENGTH OF STEEL PLATE BONDED WITH UV-CURABLE GLASS FIBER REINFORCED POLYESTER RESIN SHEET ON BOTH SIDES

*Hiroshi Higashiyama[1], Toshiyuki Ishikawa[2], Nobuhiro Mitsukawa[3], Takeshi Nagao[4] and Osamu Takahashi[4]

[1]Faculty of Science and Engineering, Kindai University, Japan; [2]Faculty of Environmental and Urban Engineering, Kansai University, Japan; [3]CTI Engineering Co., Ltd., Japan; [4]ANANDENKI Corporation, Japan

*Corresponding Author, Received: 11 Sep. 2020, Revised: 07 Nov. 2020, Accepted: 27 Jan. 2021

**ABSTRACT:** Steel structures in social infrastructures often undergo corrosion and the thickness of these steel plates decreases. Then, the strength of steel structures decreases according to the residual plate thickness. Applications of a steel plate attaching method and a fiber reinforced polymer/plastic (FRP) bonding method are effective for repair and strengthening for these steel structures. In this study, UV-curable glass fiber reinforced polyester resin (UV-GFRPR) sheet was focused instead of FRPs. The aims of this study are to confirm repair and strengthening effects of the UV-GFRPR sheet bonded on both sides of steel plate. The UV-GFRPR sheet consists of a polyester resin and chopped glass fibers and is hardened by radiation of UV source for a certain time. The tensile behavior and strength of steel plate bonded with UV-GFRPR sheets were assessed under axial tensile load. After that, the tensile behavior and strength of specimens were numerically estimated from each stress-strain curve of UV-GFRPR and steel modeled by using Menegotto-Pinto model. Furthermore, nonlinear finite element analysis (FEA) taking into account of the properties of bond layers was carried out to compare the numerical results. From the test results, the yield and ultimate strengths of specimens increased linearly according to the number of laminated layers of UV-GFRPR. Both results of the numerical calculation and the FEA agreed well with the test results. It is concluded that the numerical calculation without the contribution of bond layers can estimate the tensile behavior and strength of steel plate bonded with UV-GFRPR on both sides.

*Keywords: UV-curable polyester resin sheet, chopped glass fibers, tensile strength and behavior, non-linear FEA*

## 1. INTRODUCTION

Steel structures in social infrastructures often undergo corrosion due to environmental effects, causing a phenomenon in which the thickness decreases. As repair and strengthening for these steel structures, many researches [1-5] have been conducted on a steel plate attaching method or a fiber reinforced polymer/plastic (FRP) bonding method commonly using carbon, aramid, glass, and basalt fibers. Furthermore, “Guidelines for Repair and Strengthening of Structures using Externally Bonded FRP” has been published in Japan [6].

On the other hand, some researches have been conducted on a repair method using UV-curable resin and glass fiber fabric or chopped glass fibers [7,8]. Li et al. [7] investigated the effectiveness of UV-curable resin with glass fiber fabric to fast repair laminated beams. Peck et al. [8] investigated the mechanical performance of a FRP-joint composite pipe using UV-curable vinylester resin and chopped glass fibers. Furthermore, some researchers have used UV-curable glass fiber reinforced polymer resin (UV-GFRPR) sheet [9-14], which consists of UV-curable polyester resin and chopped glass fibers, and has excellent durability against some deterioration factors and workability in the field. However, available literature seems to be limited. Nonaka et al. [9] proposed a UV-GFRPR that satisfies the performance required against fatigue at the base of signposts and lighting poles on road bridges. Muraji et al. [10] and Ida et al. [11] adhered UV-GFRPR sheets to the stress concentrated portion at the upper end of the rib plate provided at the base of the signposts. They confirmed the effect of suppressing the propagation of fatigue cracks and extending the fatigue life. Kawarazaki et al. [12] evaluated the anti-corrosion performance and load-carrying capacity of UV-GFRPR by conducting corrosion accelerated tests and tensile tests. Mitsukawa et al. [13,14] confirmed the effect of UV-GFRPR on repair and strengthening of steel plates from tensile tests. Mitsukawa et al. [14] tested for steel coupons bonded with UV-GFRPR on one side under tensile loading. However, tensile behavior and load-carrying capacity of steel plates bonded with UV-GFRPR on both sides are not revealed so far.

In this study, to assess the effect of UV-GFRPR on repair and strengthening, steel plates bonded with a UV-GFRPR sheet of one to three laminated layers on both sides were fundamentally tested under the tensile load. The tensile behavior and strength of specimens with UV-GFRPR, and the numerical calculation and nonlinear finite element analysis (FEA) using stress-strain curves of UV-GFRPR and steel modeled are described and compared.

## 2. EXPERIMENTAL PROGRAMS

### 2.1 Materials

*2.1.1 Steel*

The steel coupons with a thickness of 3.2 mm used in this test were a type of SS400, and its mechanical properties were obtained from tensile tests using six specimens in the previous study [14] shown in Fig.1. The tensile test was conducted by a 500 kN universal testing machine and was carried out under the displacement control with a speed of 2 mm/min. The strain was measured by two strain gauges with a length of 1 mm glued on both sides of steel coupon. The displacement between the crossheads of the loading machine was also measured by a linear variable-differential transducer (LVDT) with a 50 mm capacity. The data sampling was at a speed of 2 Hz. As a dynamic measuring instrument was used in this test, the obtained strain value was less than 20,000 μ.

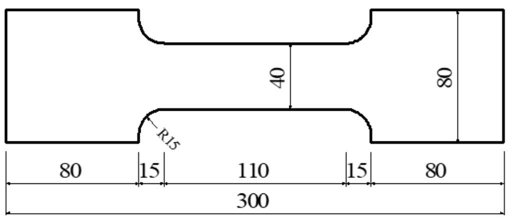


Fig.1 Shape and size of steel coupons

The stress and strain curves of the steel coupons are shown in Fig.2. Since no clear yield point was found in the test results, the yield strength was determined as 0.2% proof stress of 325 N/mm$^2$ and the tensile strength was 445 N/mm$^2$ [14].

*2.1.2 UV-GFRPR*

The UV-GFRPR used in this test was a laminated sheet which consists of a polyester resin and chopped glass fibers with a length of 25 mm. Six UV-GFRPR coupons had the same shape and dimensions as the steel coupon shown in Fig.1 were tested under the tensile load in the previous study [14]. The specimens were cut from a UV-GFRPR sheet with scissors and radiated UV source with a 40 W UV lamp for 30 min. The distance between the UV source and the specimen surface was about 50 mm. Then, the specimen thickness was about 1.6 mm. The tensile test was conducted by a 500 kN universal testing machine and was carried out under the displacement control with a speed of 0.5 mm/min. The strain was measured by two strain gauges with a length of 60 mm glued on both surfaces of UV-GFRPR coupon. The displacement between the crossheads of the loading machine was also measured by a linear variable-differential transducer (LVDT) with a 50 mm capacity. The data sampling was at a speed of 2 Hz.

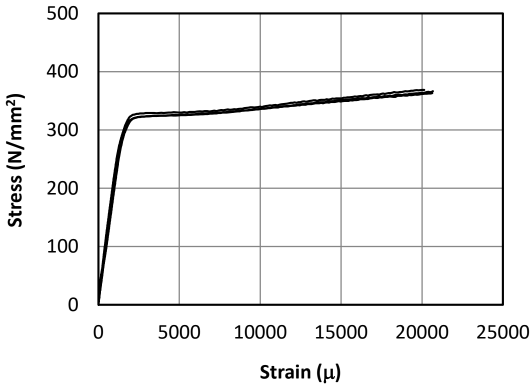


Fig.2 Stress and strain curves of steel [14]

The stress and strain curves of the UV-GFRPR coupons are shown in Fig.3. The UV-GFRPR appeared like a bi-linear behavior under the tensile stress [14]. Multiple cracks were generated in the polyester resin at a strain of about 2,000 to 2,500 μ. Then, the nonlinear relationship between the stress and the strain appeared. After that, the chopped glass fibers in the polyester resin carried the tensile stress with the bridging effect.

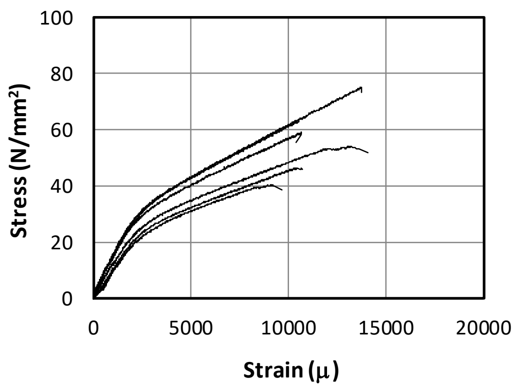


Fig.3 Stress and strain curves of UV-GFRPR [14]

Finally, a localized crack was generated from a weakest point and the specimen failed as shown in Fig.4. Overall, there is a scatter in the stress and strain curves due to the dispersion of chopped glass fiber. It is needed to consider the variation of mechanical properties of the UV-GFRPR in the future study. Using the stress and strain curve modeled by a bi-linear curve shown in Fig.5, the strengths and the Young's modulus are summarized in Table 1.

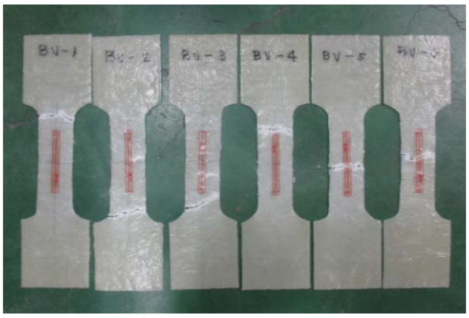

Fig.4 Failure condition of UV-GFRPR specimens after tensile loading [14]

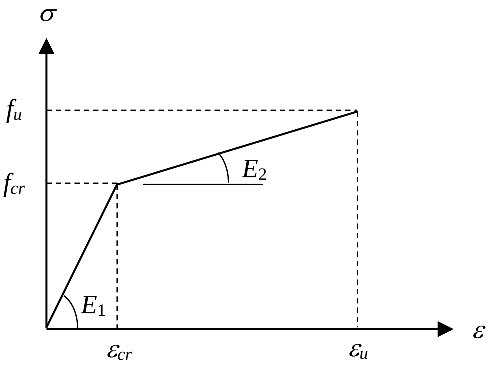


Fig.5 Schematics of stress and strain curve

Table 1 Mechanical properties of UV-GFRPR [14]

| $f_{cr}$ (N/mm$^2$) | $f_u$ (N/mm$^2$) | $E_1$ (kN/mm$^2$) | $E_2$ (kN/mm$^2$) |
|---|---|---|---|
| 29.7 | 56.3 | 11.8 | 3.1 |

### 2.2 Specimens

The specimens of steel coupons bonded with UV-GFRPR on both sides were shown in Fig.6. The hatching area in Fig.6(a) describes the bonding area of the UV-GFRPR. As the purpose of this test was to evaluate the repair and strengthening effect of the steel plate bonded with the UV-GFRPR, the bonding area of the UV-GFRPR sheet was extended to a wider part of steel coupon to avoid peeling failure of the UV-GFRPR during the test. The specimen after bonding and hardening of the UV-GFRPR sheet is shown in Fig.6(b).

The number of laminated layers was one to three on each surface of steel coupons. An acrylic resin adhesive (PEGALOCK, KOATSU GAS KOGYO, CO., LTD.) was selected to bond the UV-GFRPR sheet to steel coupons, and 400 g/m$^2$ of the acrylic resin adhesive was applied to each interface of adhesive layer. The material properties of acrylic resin adhesive from tensile tests using small coupon specimens by a manufacture, the Young's modulus, the Poisson's ratio, and the tensile strength were 3.3 kN/mm$^2$, 0.47, and 28.8 N/mm$^2$. From the density of the acrylic resin of 1.09, the thickness of each adhesive layer was calculated as 0.377 mm. The actual thickness of adhesive layer in some specimens was measured as about 0.376 mm. After the acrylic resin adhesive hardened, a 40 W UV source was radiated for 30 min at the distance of 50 mm from the specimen surface. The above manufacturing procedures were repeated for each laminated layer. For each laminated layer, three specimens were prepared.

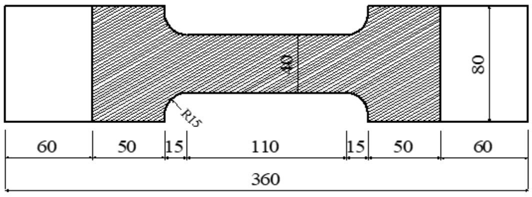


(a) Shape and size of specimens


(b) Specimens after bonded with UV-GFRPR

Fig.6 Specimens bonded with UV-GFRPR on both sides

### 2.3 Test Method

The tensile test was also conducted by a 500 kN universal testing machine and was carried out under the displacement control with a speed of 2 mm/min. The specimen was gripped at a part of the steel and the tensile force was loaded. The strain was measured by totally four strain gauges with a length of 1 mm glued on both sides of steel and a length of 60 mm glued on both surfaces of the UV-GFRPR. The displacement between the crossheads of the loading machine was also measured by a linear variable-differential transducer (LVDT) with a 50 mm capacity. The data sampling was at a speed of 2 Hz. As a dynamic measuring instrument was also used in this test, the obtained strain value was less than 20,000 μ.

## 3. RESULTS AND DISCUSSIONS

### 3.1 Tensile Behavior

*3.1.1 Stress and displacement*

The relationship between the stress and the displacement of each specimen is shown together with the result of the steel coupon in Fig.7. Here, the stress was calculated from the tensile load divided by the cross-sectional area of the steel coupon. The blue lines are the behavior of the specimens bonded with the UV-GFRPR and the black line is the behavior of the steel coupon.

The tensile behavior of the specimens bonded with the UV-GFRPR was linear beyond the yield strength of the steel coupon alone of 325 N/mm$^2$, and after the generation of multiple cracks in the UV-GFRPR, the tensile stiffness decreased. However, the stress increased until the UV-GFRPR failed due to crack localization. Then, the stress suddenly dropped and the tensile behavior was asymptotic to that of the steel coupon. Finally, the specimen reached the breakage of steel. The ultimate failure condition of specimen is shown in Fig.8.

*3.1.2 Stress and strain model of steel*

The stress and strain model including a strain hardening region of the steel is proposed by Odawara et al. [15] as shown in Fig.9. They used two curves of the Menegotto-Pinto model [16] which is represented by Eq. (1):

$$\frac{\sigma_s(\varepsilon)}{f_y} = \frac{\left(1-\frac{E_{s,\infty}}{E_s}\right)\cdot\frac{\varepsilon}{\varepsilon_y}}{\left\{1+\left(\frac{\varepsilon}{\varepsilon_y}\right)^R\right\}^{1/R}} + \frac{E_{s,\infty}}{E_s}\cdot\frac{\varepsilon}{\varepsilon_y} \qquad (1)$$

where, $\sigma_s(\varepsilon)$ is the stress of steel at a strain of $\varepsilon$, $f_y$ is the yield strength, $E_s$ is the initial Young's modulus (= 200 kN/mm$^2$), $E_{s,\infty}$ is the tangential stiffness after yielding of steel, $\varepsilon$ is the strain of steel, $\varepsilon_y$ is the yield strain (= $f_y/E_s$), $R$ is the curvature coefficient.

Regarding the curvature coefficient, $R$ in Eq. (1), $R$=7 for the first curve and $R$=0.8 for the subsequent second curve were used in this study. $E_{s,\infty}$ was set to zero similar to the result of Odawara et al. [15]. By taking the larger value of the stress obtained from these two stress and strain curves, the stress and strain curve of the steel shown in Fig.10 was obtained realistically when compared with the tensile test results of steel coupon shown in Fig.2.

*3.1.3 Stress and strain model of UV-GFRPR*

The Menegotto-Pinto model [16] was also used for the stress and strain relationship of the UV-GFRPR as shown in Fig.11. The stress and strain model is represented by Eq. (2):

$$\frac{\sigma_f(\varepsilon)}{f_{cr}} = \frac{\left(1-\frac{E_2}{E_1}\right)\cdot\frac{\varepsilon}{\varepsilon_{cr}}}{\left\{1+\left(\frac{\varepsilon}{\varepsilon_{cr}}\right)^R\right\}^{1/R}} + \frac{E_2}{E_1}\cdot\frac{\varepsilon}{\varepsilon_{cr}} \qquad (2)$$

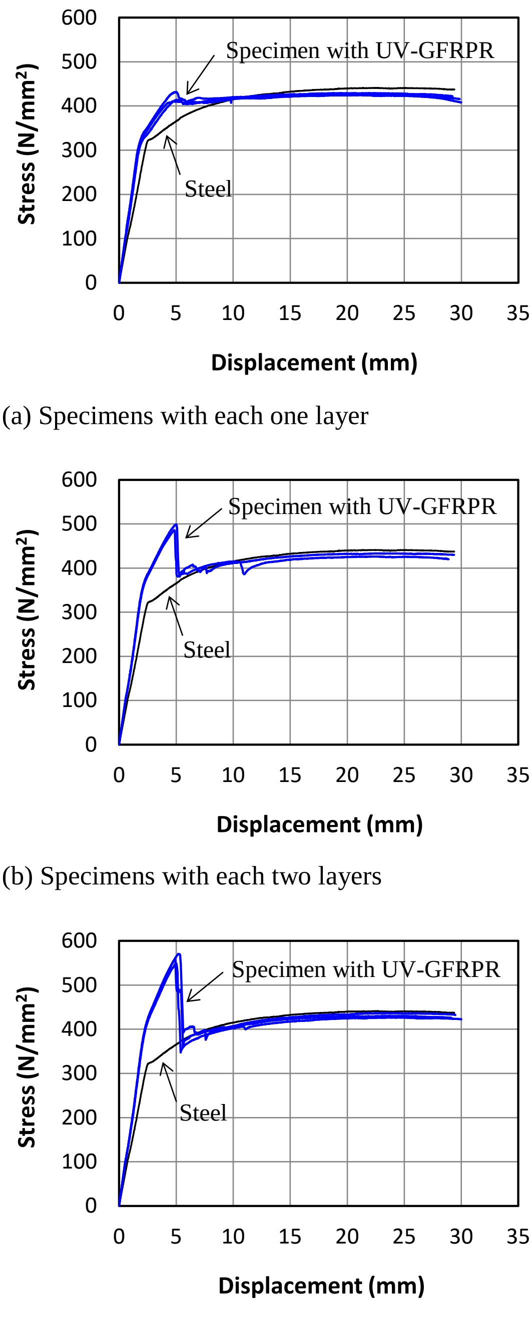


(a) Specimens with each one layer

(b) Specimens with each two layers

(c) Specimens with each three layers

Fig.7 Stress and displacement curves

where, $\sigma_f(\varepsilon)$ is the stress of UV-GFRPR at a strain of $\varepsilon$, $f_{cr}$ is the cracking strength of the UV-GFRPR, $E_1$ is the initial Young's modulus, $E_2$ is the tangential stiffness after cracking, $\varepsilon$ is the strain of UV-GFRPR, $\varepsilon_{cr}$ is the cracking strain of the UV-GFRPR ($=f_{cr}/E_1$), $R$ is the curvature coefficient.

Parameters used in Eq. (2) were the values shown in Table 1. The curvature coefficient was set to $R$=5. As a result, as shown in Fig.12, the average stress and strain relationship of the test results shown in Fig.3 can be expressed.

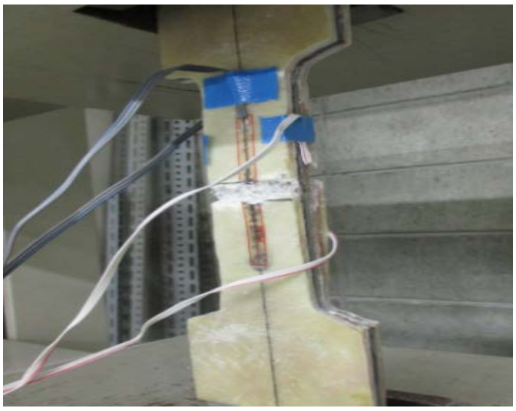

Fig.8 Ultimate failure condition

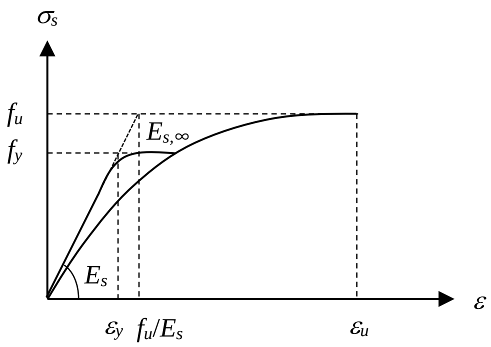


Fig.9 Stress and strain model for steel

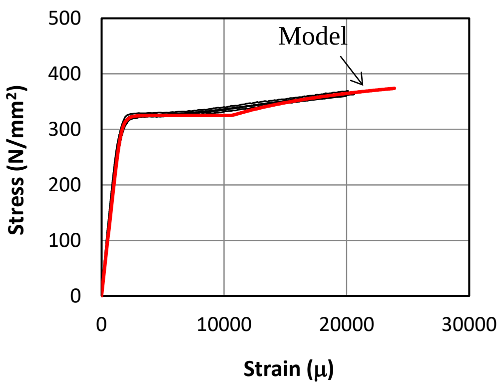


Fig.10 Comparison of stress and strain curves

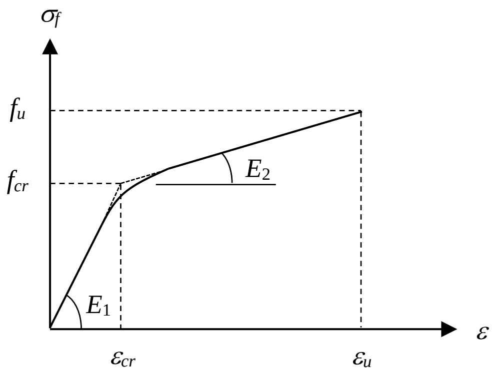


Fig.11 Stress and strain model for UV-GFRPR

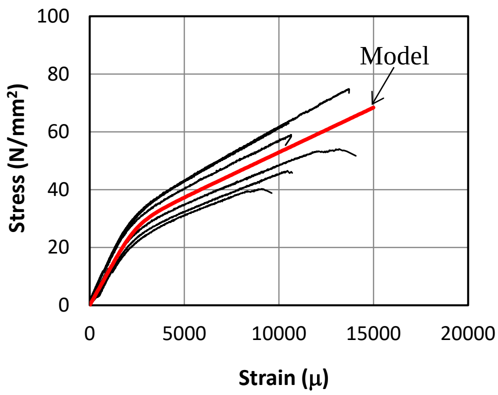


Fig.12 Comparison of stress and strain curves

*3.1.4 Prediction of tensile behavior*

From each stress and strain model of the steel and the UV-GFRPR given by Eqs. (1) and (2), respectively, the stress of steel bonded with the UV-GFRPR can be estimated by Eq. (3):

$$\sigma = \sigma_s(\varepsilon) + 2A_f\sigma_f(\varepsilon)/A_s \tag{3}$$

where, $\sigma_s(\varepsilon)$ and $\sigma_f(\varepsilon)$ are the stresses of steel and UV-GFRPR at the strain of $\varepsilon$, $A_s$ and $A_f$ are the cross-sectional areas of steel and one side of UV-GFRPR.

The stress and strain relationships calculated from Eq. (3) are plotted as red circles with the test results as shown in Fig.13 in which the strain is in the steel. From these results less than the strain of 15,000 μ, which was the strain modeled in Fig.12, the tensile behavior of specimens can be predicted well up to the strain hardening region by Eq. (3), which is simply cumulative of each steel and UV-GFRPR behavior at the same strain value. However, the behavior of the acrylic resin adhesive was ignored in this numerical calculation. Therefore, in the next section, a nonlinear FEA, in which the adhesive layer was realistically modeled, was conducted to verify the results predicted by the simple cumulative calculation model described here.

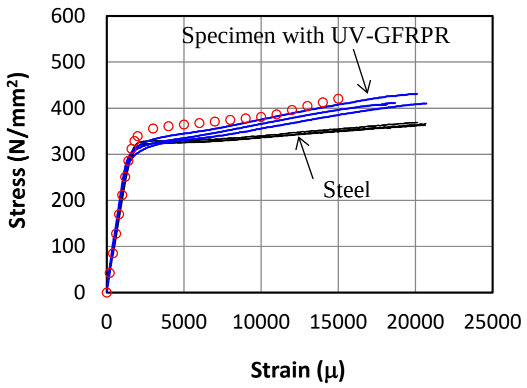


(a) Specimen with each one layer

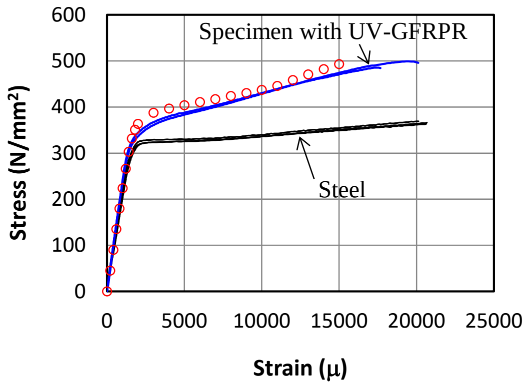


(b) Specimen with each two layers

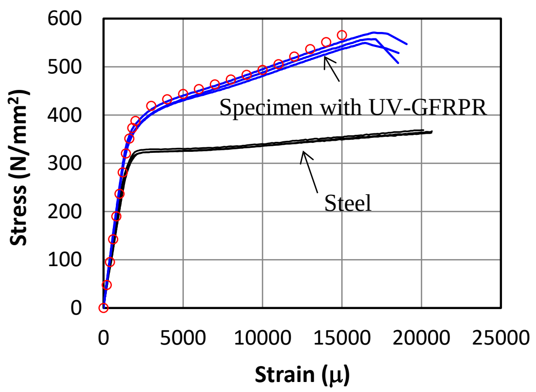


(c) Specimen with each three layers

Fig.13 Comparison of test results and calculation

## 3.2 Finite Element Analysis (FEA)

### *3.2.1 Finite element model*

To verify the tensile behavior using the simple cumulative calculation model, elastic-plastic finite element analysis using MSC. MARC software was carried out. In the analysis, the isoperimetric solid element was employed, and the one-eighth of the specimen was modeled using symmetry boundary conditions as shown in Fig.14. The material properties of steel and UV-GFRPR are same as shown in Figs.10 and 12 in the numerical calculation of tensile behavior. For the adhesive layer, the Young's modulus, the Poisson's ratio, and the thickness are assumed to be 3.3 kN/mm$^2$, 0.47, and 0.377 mm with elastic material. The nonlinear analysis was performed by applying the condition of the von Mises yield criterion and the arc length increment method.

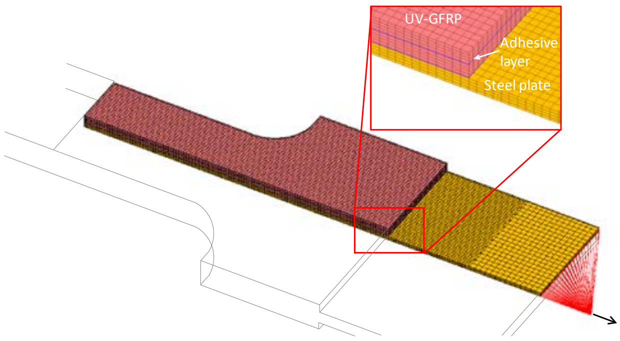


Fig.14 Finite element model

### *3.2.2 Verification of simple cumulative model*

The stress and strain relationships calculated by the FEA are shown in Fig.15 with that numerically estimated from Eq. (3). The strain in the FEA is the value on the surface of UV-GFRPR at the center of the specimen. As can be seen in Fig.15, the analytical results and the numerical results from Eq. (3) are almost same in the all cases. The influence of the acrylic resin adhesive was small in this study.

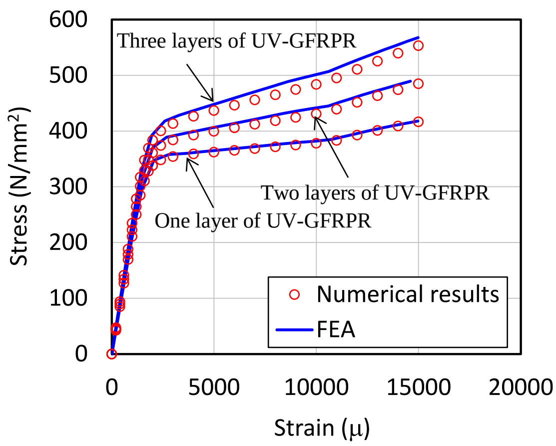


Fig.15 Comparison of numerical and FEA results

## 3.3 Tensile Strength

### *3.3.1 Yield strength and ultimate strength*

Table 2 shows the yield strength and the ultimate strength of the specimens bonded with the UV-GFRPR. The yield strength was determined from the values of the strain gauges attached to both sides of the steel as 0.2% proof stress. The ultimate strength was obtained from dividing the maximum load at the breakage of the UV-GFRPR by the cross-sectional area of the steel coupon.

From the results, the strength increasing rate based on the yield strength of the steel coupon of 325 N/mm$^2$ is shown in Fig.16. The yield strength can be expected to be few percent for one layer on both sides, over 10% for two layers on both sides, and about 30% for three layers on both sides. On the other hand, the ultimate strength can be expected to be about 30% for one layer on both sides, about 50% for two layers, and about 70% for three layers on both sides. In this study, however, the UV-GFRPR was bonded to a thin steel plate with a thickness of 3.2 mm, and it is necessary to study the effect of the difference in steel plate thickness in the future.

Table 2 Yield strength and ultimate strength

| Number of layers on each surface | Yield strength (N/mm$^2$) | Ultimate strength (N/mm$^2$) |
|---|---|---|
| One | 329 | 419 |
| Two | 368 | 492 |
| Three | 423 | 559 |

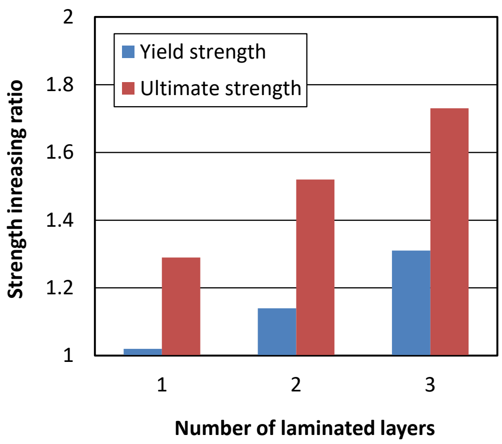


Fig.16 Strength increasing ratio based on the yield strength

*3.3.2 Cumulative strength calculation*

The yielding capacity, $N_y$, and the ultimate capacity, $N_u$, of specimens were evaluated using the following simple cumulative equations [6]:

$$N_y = A_s\sigma_s(\varepsilon_y) + 2A_f\sigma_f(\varepsilon_y) \quad (4)$$

$$N_u = A_s\sigma_s(\varepsilon_{fu}) + 2A_f\sigma_f(\varepsilon_{fu}) \quad (5)$$

where, $A_s$ and $A_f$ are the cross-sectional areas of steel and one side of UV-GFRPR, $\sigma_s(\varepsilon_y)$ and $\sigma_f(\varepsilon_y)$ are the stresses of steel and UV-GFRPR at the yield strain of steel, $\sigma_s(\varepsilon_{fu})$ and $\sigma_f(\varepsilon_{fu})$ are the stresses of steel and UV-GFRPR at the rapture of UV-GFRPR.

In the calculation of tensile capacities from Eqs. (4) and (5), the yield strain of steel was 1,625 μ from the yield strength of steel of 325 N/mm$^2$ and the Young's modulus of 200 kN/mm$^2$. The rupture strain of UV-GFRPR was 11,200 μ as the average value obtained from the tensile test shown in Fig.3. Table 3 shows the results of a comparison between the test values and the calculated values for the tensile capacities of the test specimens at the time of steel yielding and UV-GFRPR fracture. The yielding capacity was accurately evaluated for each number of layers. On the other hand, for the ultimate capacity, the calculated values at breakage of UV-GFRPR were underestimated by about 10% regardless of the number of layers. The cause of underestimation might be the determination of the rupture strain of UV-GFRPR.

Table 3 Comparison of tensile capacities

| No. of layers on each surface | Yielding capacity, $N_y$ | | |
|---|---|---|---|
| | $N_{y,\,test}$ (kN) | $N_{y,\,cal.}$ (kN) | $\frac{N_{y,\,test}}{N_{y,\,cal.}}$ |
| One | 37.8 | 39.3 | 0.96 |
| Two | 38.6 | 41.8 | 0.92 |
| Three | 45.3 | 44.2 | 1.02 |
| No. of layers on each surface | Ultimate capacity, $N_u$ | | |
| | $N_{u,\,test}$ (kN) | $N_{u,\,cal.}$ (kN) | $\frac{N_{u,\,test}}{N_{u,\,cal.}}$ |
| One | 52.7 | 49.0 | 1.08 |
| Two | 61.5 | 56.5 | 1.09 |
| Three | 70.6 | 64.1 | 1.10 |

## 4. CONCLUSIONS

In this study, the thin steel plates bonded with the UV-GFRPR sheets on both sides were tested under the tensile stress. From the results on the fundamental tests, numerical calculation, and FEA, the following conclusions can be drawn.

The tensile behavior of the specimens bonded with the UV-GFRPR was linear beyond the yield strength of the steel coupon alone, and after the generation of multiple cracks in the UV-GFRPR, the tensile stiffness decreased. However, the stress increased until the UV-GFRPR failed due to crack localization. Then, the stress suddenly dropped and the tensile behavior was asymptotic to that of the steel coupon.

The simple cumulative calculation model was used to predict the tensile behavior of the specimens.

Then, the stress and strain relationships on the specimens bonded with the UV-GFRPR were able to be predicted well up to the breakage of UV-GFRPR. Furthermore, the validity of the model was confirmed to compare the results of the FEA. Then, both results were in good agreement.

The yield and ultimate strengths increased linearly with the number of laminated layers. Based on the yield strength of the steel coupon, the yield strength can be expected to be few percent for one layer on both sides, over 10% for two layers on both sides, and about 30% for three layers on both sides.

The yielding and ultimate capacities were also evaluated using the simple cumulative calculation. The yielding capacity at steel yield was accurately evaluated for each number of layers. On the other hand, for the ultimate capacity, the calculated values at breakage of UV-GFRPR were underestimated by about 10% regardless of the number of layers.

## 5. REFERENCES

[1] Zhao X.L. and Zhang L., State-of-the-art Review on FRP Strengthened Steel Structures, Engineering Structures, Vol. 29, No. 8, 2007, pp. 1808-1823.

[2] Hollaway L.C., A Review of the Present and Future Utilization of FRP Composites in the Civil Infrastructure with Reference to Their Important In-service Properties, Construction and Building Materials, Vol. 24, 2010, pp. 2419-2445.

[3] Teng. J.G., Yu T. and Fernando D., Strengthening of Steel Structures with Fiber-reinforced Polymer Composites, Journal of Constructional Steel Research, Vol. 78, No. 11, 2012, pp. 131-143.

[4] Silva M.A.G., Biscaia H. and Ribeiro P., On factors affectin CFRP-steel bonded joints, Construction and Building Materials, Vol. 226, 2019, pp. 360-375.

[5] Jayasuriya S., Batani A., Kenno S., Bolisetti, T. and Das S., Rehabilitation of Corroded Steel Beams Using BFRP Fabric, Structures, Vol. 15, 2018, pp.152-161.

[6] Japan Society of Civil Engineers, Guidelines for Repair and Strengthening of Structures using Externally Bonded FRP, Hybrid Structure Series 09, 2018, pp. 1-274.

[7] Li G., Pourmohamadian N., Cygan A. and Peck J., Fast Repair of Laminated Beams Using UV Curing Composites, Composite Structures, Vol. 60, 2003, pp. 73-81.

[8] Peck J.A., Jones R.A., Pang S.S., Li G. and Smith B.H., UV-cured FRP joint thickness effect on coupled composite pipes, Composite Structures, Vol. 80, 2007, pp. 290-297.

[9] Nonaka S., Ida T., Muraji S. and Hirano H., Repair and Reinforcement with UV Curable FRP Sheet Utilizing Material Properties, The 57th Annual Conference of JSCE, I-298, 2020, pp. 595-596 (in Japanese).

[10] Muraji S., Hirano H., Aoki T., Ida T., Yong Y. and Matsui K., Experiments in Longevity Materials with “UV-Curable-FRP-SHEET” on Pillar Structures, Journal of JSCE, No. 784/VI-66, 2005, pp. 99-107 (in Japanese).

[11] Ida T., Hirano H., Matsui K. and Muraji S., Study of Fatigue Improvement by “UV-Curable-FRP-SHEET-Reinforcement”, Journal of Applied Mechanics, Vol. 9, 2006, pp. 1085-1092 (in Japanese).

[12] Kawarazaki Y., Manebe Y., Mitsukawa N., Muranaka A., Nakamura I., Nagao T. and Mayuzumi Y., Study on Repair of Steel Member Using UV-Curable Polyester Resin GFRP Sheet, The 72th Annual Conference of JSCE, V-489, 2017, pp. 977-978 (in Japanese).

[13] Mitsukawa N., Manabe Y., Kawarazaki Y., Takahashi O., Nagao T., Muranaka A. and Nakamura I., Study on Reinforcement of Steel Member Using UV-Curable Polyester Resin GFRP Sheet, The 73th Annual Conference of JSCE, VI-283, 2018, pp. 565-566 (in Japanese).

[14] Mitsukawa N., Nagao T., Takahashi O., Higashiyama H. and Ishikawa T., Tensile Properties of Steel Plate Bonded with UV-Curable Polyester Resin GFRP Sheet, Proceedings of The Sixth International Conference on Construction Materials, Fukuoka, 2020, pp. 525-532.

[15] Odawara K., Bai Y., Kawano A. and Matsuo S., Stress-Strain Model of Structural Members by Considering Strength Degradation (Part.2 Steel and Reinforced Concrete Structural Members), Proceedings of The 9th Symposium on Research and Application of Hybrid and Composite Structures, 2011, pp. 193-202.

[16] Menegotto M. and Pinto P.E., Method of Analysis for Cyclic Loaded RC Frames Including Changes in Geometry and Non-Elastic Behavior of Elements under Combined Normal Force and Bending, Proc. of IABSE symposium on Resistance and Ultimate Deformation of Structures Acted on by Well Defined Repeated Loads, 1973, pp. 15-22.